Regulatory effects of the long non-coding RNA RP11-543N12.1 and microRNA-324-3p axis on the neuronal apoptosis induced by the inflammatory reactions of microglia

MIAO CAI*, YAN-WEN WANG*, SHAN-HU XU, SONG QIAO, QIN-FEN SHU, JIAN-ZONG DU, YA-GUO LI and XIAO-LI LIU

Department of Neurology, Zhejiang Hospital, Hangzhou, Zhejiang 310013, P.R. China

Received September 6, 2017; Accepted June 15, 2018

DOI: 10.3892/ijmm.2018.3736

Abstract. The present study aimed to examine how the long non-coding RNA (lncRNA) RP11-543N12.1 interacted with microRNA (miR)-324-3p to modify microglials (MIs)-induced neuroblastoma cell apoptosis, which may pose benefits to the treatment of Alzhemier's disease (AD). The cell model of AD was established by treating SH-SY5Y cells with amyloid β $(Aβ)_{25-35}$, and MI were acquired using primary cell culture technology. The lncRNAs that were differentially expressed between SH-SY5Y and control cells were screened through a microarray assay and confirmed via polymerase chain reaction. In addition, overexpression of RP11-543N12.1 and miR-324-3p was established by transfection of SH-SY5Y cells with pcDNA3.1(+)-RP11-543N12.1 and miR-324-3p mimics, respectively, while downregulation of RP11-543N12.1 and miR-324-3p was achieved by transfection with RP11-543N12.1-small interfering RNA (siRNA) and miR-324-3p inhibitor, respectively. The interaction between RP11-543N12.1 and miR-324-3p was confirmed with a dual-luciferase reporter gene assay. The results revealed that the expression levels of total and phosphorylated tau in SH-SY5Y cells were significantly elevated following $Aβ_{25-35}$ treatment (P<0.05), and RP11-543N12.1 was found to be differentially expressed between the control and Aβ25-35-treated cells (P<0.05). Furthermore, the targeted association of RP11-543N12.1 and miR-324-3p was predicted based on miRDB4.0 and PITA databases, and then validated via the dual-luciferase reporter gene assay. SH-SY5Y cells transfected with siRNA or inhibitor, and treated with $Aβ_{25-35}$ displayed cellular survival and apoptosis that were similar to the normal levels (P<0.05). Finally, co-culture of MI and SH-SY5Y cells transfected with RP11-543N12.1-siRNA/miR-324-3p inhibitor significantly enhanced cell apoptosis (P<0.05). In conclusion, RP11-543N12.1 targeted miR-324-3p to suppress proliferation and promote apoptosis in the AD cell model, suggesting that RP11-543N12.1 and miR-324-3p may be potential biomarkers and therapeutic targets for AD.

Correspondence to: Dr Xiao-Li Liu, Department of Neurology, Zhejiang Hospital, 12 Lingyin Road, Xihu, Hangzhou, Zhejiang 310013, P.R. China
E-mail: docterxiaoliliu@yeah.net

*Contributed equally

Key words: Alzheimer's disease, microglia, long non-coding RNA, RP11-543N12.1, microRNA-324-3p, cellular apoptosis

Introduction

Alzheimer's disease (AD) is characterized by the presence of neurofibrillary tangles and neuron loss, which are generated by amyloid β (Aβ)-induced plaques and abnormally aggregated hyperphosphorylated tau (1,2). AD onset, which features progressively dysfunctional cognition and pathological neuron loss, is considered to be associated with the activation of neuroinflammatory factors, astrocytes, microglia (MI) and the complement system (3). A total of ~5% of the worldwide population >65-years old are at risk of developing AD, and ≤30% population aged >85-years-old suffer from AD, emphasizing the evidently incremental trend of AD patients with aging (4). Since late-stages of AD are accompanied with dementia and gradual loss of self-sufficiency, it is important that AD patients are diagnosed and treated at the mild or moderate stages of the disease (5). Various drug therapies for AD have been emerging, including cholinesterase inhibitors (such as donepezil) and N-methyl-D-aspartic acid receptor antagonists (such as memantine hydrochloride). Nevertheless, these therapies merely delay cognitive decline, rather than prohibiting the progression of AD. Thus, it is urgent to explore the pathogenesis of AD in order to facilitate the development of novel diagnostic biomarkers and efficient treatment targets for this disease.

Certain long non-coding RNAs (lncRNAs) are differentially expressed within astrocytes, oligodendrocytes and glia, indicating that they may participate in the pathogenesis of certain neuronal disorders by acting on downstream microRNAs (miRs) and mRNAs (6). For instance, lncRNA SNHG14 may result in activated MI via modifying downstream miR-145-5p and PLA2G4A, elevating the probability of an individual suffering from cerebral infarction (7). Furthermore,

the lncRNA *2700046G09Rik*/miR-23a/phosphatase and tensin homolog axis served a crucial role in the myelination process of oligodendrocytes (8), while lncRNA MEG3 interacted with miR-181b to interfere with anoxia-induced neuronal apoptosis (9).

The abnormal expression of certain miRNAs has been documented to be implicated in the etiology of AD, including miR-146a, miR-34a, miR-125a and miR-324-3p (10). For instance, miRNA-34a within activated MI was associated with Aβ accumulation by inhibiting Trem-2 expression (11), while the pro-inflammatory responses of MI were also subject to the modulation of miR-146a within AD mice brains (12). Furthermore, miR-324-3p was able to mediate the expression of Rel A (13,14), which participates in neuritis growth and apoptosis (15,16). Thus, it was suggested that miR-324-3p may modulate neuronal growth or apoptosis, and aberrant functioning of this miRNA may be involved in triggering AD development. Considering the interactive role of lncRNAs and miRNAs in promoting numerous diseases, the present study was conducted to determine an lncRNA/miRNA axis that may partly account for AD development.

It is also notable that the increased Aβ dimers due to AD onset damage the synaptic plasticity (17), and thereby lead to neuritic abnormalities (1). During this process, the abnormally induced Aβ under pathological conditions may activate the MI cells, reducing Aβ levels and producing inflammatory factors, thus inducing damage and the apoptosis of neurons (18). As a result, it was further hypothesized that the lncRNA/miRNA axis proposed by the current study may interfere with MI-induced neuronal apoptosis.

Overall, the aim of the present study was to identify a potentially significant lncRNA and its targeted miRNA underlying AD pathogenesis via chip hybridization analysis, which may provide a foundation for the diagnosis and treatment of early-stage AD.

Materials and methods

Culture, purification and passage of MI. After the written approval of a female participant and the ethics committee of Zhejiang Hospital (Hangzhou, China) were acquired, the fetus whose life was terminated around 12 weeks after pregnancy was taken from the obstetrics and gynecology department of Zhejiang hospital (Zhejiang province, China). In accordance with the methods reported by Dobrenis *et al* (19), the 12-week aborted fetus was washed with tri-distilled water, and was then soaked in 75% alcohol for 5 min. Following washing with PBS, the embryo was decapitated under a dissecting microscope, and the skull was sectioned to collect the brain tissues (cortex and medulla). The meninges and blood vessels were removed, and cold DMEM was prepared to rinse the brain tissues. Then the tissues were mechanically dissociated with a pipette (1-ml), and 0.25% trypsin was added for 15-min digestion at 37˚C. Subsequently, 10% PBS was added to terminate digestion, and the mixtures were filtered via a 200-mesh sieve. The obtained filtrate was collected for 100 x g centrifugation at room temperature for 5 min, and then the supernatant was discarded. Additionally, DMEM medium that contained 10% FBS was added, and single-cell suspension was consequently made following mechanical isolation of the samples. Then the cells at a density of $1x10^5$/ml were inoculated into an air-permeable culture flask that was pre-coated with poly-lysine. Subsequently, cells were cultured under in 5% CO_2 and 95% air at 37˚C. After 2 days, cell growth and survival were observed for 7-9 days, and medium was changed every 3-4 days.

After 7-9 days of culture, at room temperature, the samples were agitated at 26 x g for 2 h prior to removal of the supernatant. Finally, the MI-containing culture solution was transferred to a poly-lysine-coated culture plate for 30-min cultivation in 5% CO_2 at 37˚C. When cells grew to cover the well plate, they were digested with pancreatin for subculture; passage 4 was used for subsequent analysis. With addition of CD11b antibody (1:100; Y07D10A; Wuham Boster Biological Technology, Ltd., Wuhan, China), MIs were identified according to the instructions of DAB staining kit (08A04A22; Wuhan Boster Biological Technology, Ltd.) (20). The purified MIs were stained with 1% cresyl-violet (Nanjing SenBeiJia Biological Technology, Nanjing, Jiangsu Province, China) at 37˚C for 20 min, and they were also managed with CD68 immuno-fluorescent staining (OriGene Technologies, Inc., Rockville, MD, Beijing, China). A total of 20 views per field were collected to calculate number of cresyl violet-stained or CD68-positive cells, and the purity of MI was calculated according to the formula of $N_{CD68+}/N_{cresyl\ violet+}$.

Construction of AD cell models. Human neuroblastoma SH-SY5Y cells were purchased from the Cell Bank of the Chinese Academy of Sciences (Shanghai, China) and cultured in high-glucose Dulbecco's modified Eagle's medium (DMEM) (Thermo Fisher Scientific, Inc., Waltham, MA, USA), which included 10% fetal bovine serum (FBS; Gemini Bio Products, West Sacramento, CA, USA), 100 U/ml penicillin (Thermo Fisher Scientific, Inc.) and 0.1 mg/ml streptomycin (Thermo Fisher Scientific, Inc.) under saturated humidity in 5% CO_2 at 37˚C. For the AD cell model group, $A\beta_{25-35}$ (Sigma-Aldrich; Merck KGaA, Darmstadt, Germany) was added to the cells at the logarithmic growth phase, and the final concentration of $A\beta_{25-35}$ was adjusted to 20 μmol/l. For the control group, the cells at the logarithmic growth phase were treated with 10% dimethyl sulfoxide. The aforementioned AD cell model and control group were both incubated at 37˚C for another 48 h, and each of them was managed with six repeats. Three of the repeats were used for the detection of P-tau in order to verify whether the AD cell model was successfully established, and the other three repeats were prepared for microarray data analysis (KangCheng Biological Engineering, Shanghai, China).

Separation of nucleus from cytoplasm. Nuclear/cytoplasmic separation of SH-SY5Y cells was implemented using the PARIS™ Protein and RNA Isolation System kit (Thermo Fisher Scientific, Inc., Waltham, MA, USA). The 45S ribosomal RNA (rRNA) was set as the internal reference for nucleus RNAs, and 12S rRNA was designated as the internal reference for cytoplasmic RNAs.

Chip hybridization and data analysis. Sample labeling and chip hybridization were performed for the aforementioned AD and control cells groups, according to the protocols of Agilent One-Color Microarray-Based Gene Expression Analysis

Table I. Primers for RP11-543N12.1-siRNA, RP11-543N12.1 and β-actin.

Genes	Primers
RP11-543N12.1-siRNA	
siRNA-1	5'-CCAGCAGAUUAGUCUGCAUTT-3' (sense)
	5'-AUGCAGACUAAUCUGCUGGTT-3' (antisense)
siRNA-2	5'-GGGAUGGUCACCUGUAAAUTT-3' (sense)
	5'-AUUUACAGGUGACCAUCCCTT-3' (antisense)
siRNA-3	5'-GAUGGACCACGUUGAGCAUTT-3' (sense)
	5'-AUGCUCAACGUGGUCCAUCTT-3' (antisense)
RP11-543N12.1	5'-CAAGACTAGCGTCTCCCAGC-3' (forward)
	5'-GTCTTGGTGCATTTGATTTCTCTGA-3' (reverse)
β-actin	5'-GAAGTGTGACGTGGACATCC-3' (forward)
	5'-CCGATCCACACGGAGTACTT-3' (reverse)

(Agilent Technologies, Inc., Beijing, China). Specifically, TRIzol reagent (Invitrogen; Thermo Fisher Scientific, Inc.) was employed to extract total RNA from the cells. The mRNAs were obtained by removing rRNA from total RNA (mRNA-ONLYTM Eukaryotic mRNA Isolation; Epicentre, Madison, WI, USA), and were amplified following the random primer method (21). The amplified mRNAs underwent reverse transcription (RT) into cDNAs at 42˚C for 60 min, according to the guidance of PrimeScript™ RT reagent kit (RR037B; Takara Bio, Inc., Otsu, Japan). The cDNAs were then transcribed into fluorescent cRNAs with aid of T7 RiboMAX™ Express RNAi System (P1700; Promega Corporation). Subsequently, the labeled cRNAs were purified utilizing the RNeasy Mini Kit (Qiagen GmbH, Duesseldorf, Germany), and Nanodrop ND-1000 (Thermo Fisher Scientific, Inc.) was used to detect their concentration and activity. Subsequently, cRNAs were precipitated with absolute ethanol and dried prior to being dissolved in 16 μl hybridization solution (15% methanamide, 0.2% SDS, 3X SSC and 50X Denhardt's) at 42˚C overnight (Agilent Technologies, Inc., Santa Clara, CA, USA). After completion of chip hybridization, the chips were washed, fixed and scanned with a DNA microarray Scanner (G2505C; Agilent Technologies, Inc.). The Agilent Feature Extraction software (version 11.0.1.1) was applied to read the chip values, which were then processed via GeneSpring GX version 12.1 software (both from Agilent Technologies, Inc.). Notably, the values that demanded standardizing were further analyzed following screening of high-quality probes, and the ratio of the P-value and false discovery rate was determined to select the differentially expressed lncRNAs or mRNAs. Furthermore, hierarchical clustering and association analysis were conducted via compiling scripts.

RT-quantitative polymerase chain reaction (RT-qPCR). SH-SY5Y cells were inoculated into 6-well plates at the density of $4.5x10^5$ cells/ml. When cell confluence reached about 50%, cells were treated with $A\beta_{25-35}$. After ~48 h, total RNA was extracted with usage of TRIzol® reagent (Invitrogen; Thermo Fisher Scientific, Inc.). The purity (A260 nm/A280 nm) and concentration of RNA were determined spectrophotometrically. Next, total RNA was reverse transcribed into cDNA, with assistance of 10 μl RT mixture (Sigma-Aldrich; Merck KGaA), which included 2 nt 10X RT buffer, 1 μl RT Enzyme Mix, 2 μl FQ-RT Primer Mix and RNase-Free ddH_2O. The reverse transcription conditions involved incubation at 42˚C for 15 min, and then at 95˚C for 3 min. Subsequently, the products were subjected to qPCR analysis with THUNDERBIRD SYBR® qPCR Mix (Toyobo Life Science, Osaka, Japan). The reaction system (20 μl) was made up of cDNA template (2 μl), 10 μM forward primer (1 μl), 10 μM reverse primer (1 μl), 2X SuperReal PreMix Plus (10 μl) and RNase-free H_2O. The CFX96 Touch Real-Time PCR detection system (Bio-Rad Laboratories, Inc., Hercules, CA, USA) was used, and the qPCR reaction conditions were as follows: Pre-degeneration at 95˚C for 30 sec, 39 cycles of degeneration at 95˚C for 5 sec, followed by annealing and extension at 58-60˚C for 32 sec. The $2^{-\Delta\Delta Cq}$ method (22) was employed to analyze the relative expression levels of lncRNA and mRNA, with β-actin serving as the internal reference. All the primers were synthesized by Sangon Biotech Co., Ltd. (Shanghai, China) and are listed in Table I.

Western blotting. Total protein was extracted from the cells utilizing SDS lysis buffer (Beyotime Institute of Biotechnology, Shanghai, China), and Bradford's method was conducted to measure the concentration of total protein. The proteins were separated by 8% SDS-PAGE, and then the samples were transferred to a polyvinylidene fluoride (PVDF) membrane. Subsequently, the PVDF membrane was blocked at room temperature in Tris-buffered saline Tween-20 (TBST) that contained 5% skim milk powder for 1 h. Subsequently, primary antibodies were added, including rabbit anti-mouse tau primary antibody (1:1,000; ab64193; Abcam, Cambridge, MA, USA), rabbit anti-mouse tau-S404 primary antibody (1:1,000; ab92676; Abcam), rabbit anti-mouse tau-T231 primary antibody (1:1,000; ab151559; Abcam), rabbit anti-mouse GAPDH primary antibody (1:200; Abcam), rabbit anti-mouse p53 monoclonal antibody (1:200; ab31333; Abcam), rabbit anti-mouse B-cell lymphoma-2 (Bcl-2) monoclonal antibody (1:100; ab182858; Abcam) and rabbit

anti-mouse Bcl-2-associated X (Bax) monoclonal antibody (1:200; ab2568; Abcam). Following incubation overnight at 4˚C and rinsing with TBST, goat anti-rabbit horseradish peroxidase-conjugated IgG (HRP-IgG) (1:2,000; ab6721; Abcam) were added for incubation at 37˚C for a further 1 h. Based on the manufacturer's protocols of ECL chemi-luminescence assay kit (Beyotime Institute of Biotechnology), color development was completed. Finally, the integrated optical density (IOD) of protein bands was measured by the Lab Works 4.5 image acquisition instrument (Syngene Europe, Cambridge, UK), and the GAPDH protein bands were designated as the internal reference.

Construction of pcDNA3.1(+)-RP11-543N12.1 vector and lentiviral transfection. With assistance of T_4 DNA ligase (Fermentas Thermo Fisher, Scientific, Inc.), the PCR products of RP11-543N12.1 were inserted into the eukaryotic expression vectors pcDNA3.1(+) that were digested by two restriction enzymes of *Eco*RI (Fermentas; Thermo Fisher Scientific, Inc.) and *BamH*I (Fermentas; Thermo Fisher Scientific, Inc.). Then the ligated products were transformed into DH5a competent cells (Shanghai GeneChem, Co., Ltd., Shanghai, China), which were then spread onto plates for 37˚C culture. Subsequently, the supernatant was collected for the following transfection of SH-SY5Y cells. Furthermore, according to the instructions of the lentivirus packaging kit (BBV0017; Backer Biotech Zhengzhou, China), the double enzyme vector pGLV was co-transfected into SH-SY5Y cells with pHelper 1.0 and pHelper 2.0, and cell supernatants that were rich in lentiviral particles were collected by 100 x g centrifugation at room temperature for 10 min. In addition, RP11-543N12.1-siRNA sequences were designed and synthesized by Shanghai GenePharma Co., Ltd. (Shanghai, China). The sense and anti-sense sequences were as follows: siRNA1#, sense 5'-CCA GCAGAUUAGUCUGCAUTT-3', antisense 5'-AUGCAG ACUAAUCUGCUGGTT-3'; siRNA2#, sense 5'-GGGAUG GUCACCUGUAAAUTT-3', antisense, 5'-AUUUACAGG UGACCAUCCCTT-3', and siRNA3#, sense 5'-GAUGGA CCACGUUGAGCAUTT-3', and 5'-AUGCUCAACGUG GUCCAUCTT-3'. The SH-SY5Y cells at the logarithmic growth phase were employed for transfection process using Lipofectamine 2000 (Invitrogen; Thermo Fisher Scientific, Inc.).

The SH-SY5Y cells transfected with RP11-543N12.1-siRNA were grouped as follows: i) MOCK; ii) MOCK+A$\beta_{25\text{-}35}$ (20 μmol/l); iii) negative control (NC); iv) NC+A$\beta_{25\text{-}35}$ (20 μmol/l); v) RP11-543N12.1-siRNA and vi) RP11-543N12.1-siRNA+A$\beta_{25\text{-}35}$ (20 μmol/l). Furthermore, the cells transfected with RP11-543N12.1-overexpressed plasmids were divided into: i) MOCK; ii) MOCK+A$\beta_{25\text{-}35}$ (20 μmol/l); iii) pcDNA3.1(+); iv) pcDNA3.1(+)+A$\beta_{25\text{-}35}$ (20 μmol/l); v) pcDNA3.1(+)-RP11-543N12.1; and vi) pcDNA3.1(+)-RP11-543N12.1+A$\beta_{25\text{-}35}$ (20 μmol/l). The afore-mentioned cells were cultured at room temperature for 48 h, after being treated with 20 μmol/l A$\beta_{25\text{-}35}$ at room temperature for 48 h. The RP11-543N12.1-siRNA sequence employed in the present study was designed and synthesized by Shanghai GenePharma Co., Ltd. In addition, miR-324-3p inhibitor and miR-324-3p mimic were purchased from Biomics Biotechnologies (Nantong, Jiangsu Province, China).

Target prediction. The software MIRDB4.0 (http://mirdb.org/miRDB/index.html) and PITA (http://genie.weizmann.ac.il/pubs/mir07/mir07_exe.Html) were operated to co-predict the target miRNAs of lncRNA RP11-543N12.1.

Dual-luciferase reporter assay. The RP11-543N12.1 fragment that contained binding sites for miR-324-3p was amplified and cloned into the psiCHECK-2 luciferase vector (Promega, Madison, WI, USA), and the resultant was termed RP11-543N12.1-wild-type (wt). Next, the binding sites within the RP11-543N12.1 fragment were mutated using an XL Site-directed Mutagenesis kit (Qiagen, Duesseldorf, Germany), and the obtained fragment was connected with luciferase vectors to construct RP11-543N12.1-mutated (mut). With assistance of Lipofectamine 2000 (Invitrogen, Carlsbad, CA, USA), miR-324-3p mimic or miR-NC was co-transfected with RP11-543N12.1-wt or RP11-543N12.1-mut into SH-SY5Y cells. The activities of reporter genes were detected with the Dual-Luciferase Reporter Assay kit (Promega Corporation), and analyzed by means of Turner Designs Spreadsheet Interface (version 2.0.1; Turner Designs, Sunnyvale, CA, USA).

Establishment of the transwell co-culture system. A transwell chamber was devised as the culture device: The upper chamber was arranged for the inoculation of MI, while the lower chamber was prepared for cultivation of SH-SY5Y cells. The concentrations of SH-SY5Y cells and MI were adjusted to $1.0x10^6$/ml, respectively, with DMEM and F12 that contained 10% FBS. The specific grouping and treatment details were described as follows: i) NC group, in which SH-SY5Y cells ($1.0x10^6$/ml) were cultured within the lower chamber, with 2 ml medium added in the upper chamber; ii) Aβ stimulation group, in which SH-SY5Y cells were cultured in the lower chamber and 10 μM A$\beta_{25\text{-}35}$ was added into the upper chamber; iii) MI stimulation group, in which SH-SY5Y cells and MI were, respectively, inoculated in the lower and upper chambers according to the concentration ratio of 1:1; and iv) Aβ and MI co-stimulation group, in which the same treatment as that of the MI stimulation group was performed, with addition of 10 μM A$\beta_{25\text{-}35}$ into the MI layer subsequent to attachment of MI cells onto the plate wall. The aforementioned cell groups were all cultured in 5% CO_2 at 37˚C for 96 h, and the incubation time was counted from the addition of A$\beta_{25\text{-}35}$. Approximately five repeats of each group were conducted.

Detection of SH-SY5Y cell survival rate with an MTT assay. SH-SY5Y cells were seeded into 96-well plates at the density of 5,000/well, and 200 ml antibiotic-free medium was added in each well. At the time points of 0, 24, 48 and 72 h, each well was added with 5 g/l MTT (20 μl). Subsequent to culturing for 4 h, 150 μl dimethyl sulfoxide was added to each well and shaken for 10 min. Finally, the optical density (OD) values at 490 nm were measured with a universal microplate spectrophotometer, and the cell survival rate was calculated according to the following formula: $OD_{experimental\ group}/OD_{control\ group}$ x 100%.

Detection of SH-SY5Y cell apoptosis with the Annexin V-FITC/propidium iodide (PI) method. The apoptotic status of SH-SY5Y cells was determined with the

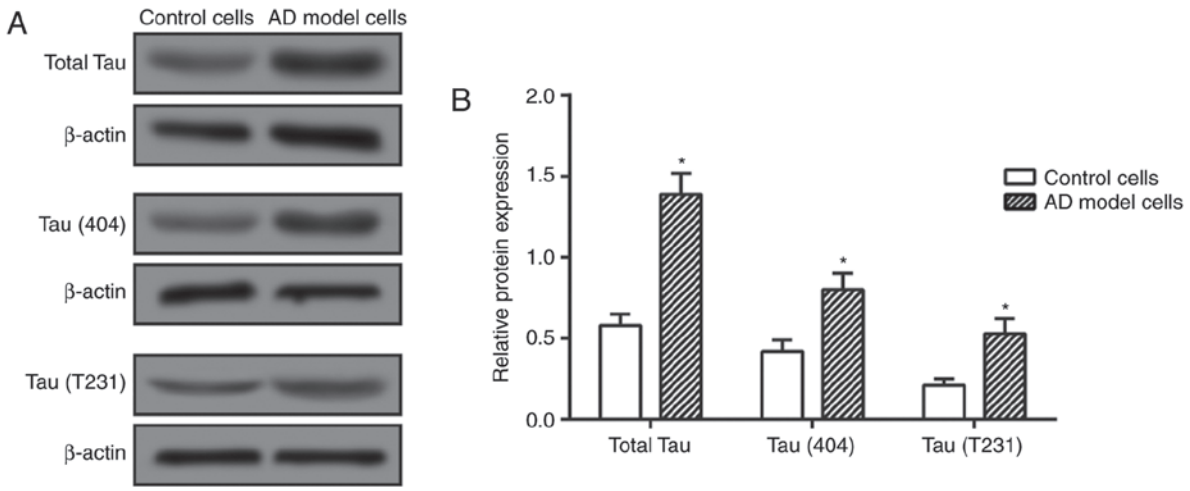

Figure 1. Protein expression levels of total tau, tau (S404) and tau (T231) between the AD cell model and normal cell groups were examined by western blot analysis and are presented as (A) protein bands and (B) bar graphs. *P<0.05 vs. the respective control group. AD, Alzheimer's disease.

Annexin V-FITC/PI apoptosis detection kit (Beyotime Institute of Biotechnology). Briefly, after cells were rinsed twice with PBS, binding buffer (100 μl) and 20 μg/ml FITC-labeled Annexin V (10 μl) were added, and the mixture was kept in the dark at room temperature for 30 min. Subsequently, the mixture was supplemented with 50 μg/ml PI (5 μl) and 400 μl binding buffer. A sample without Annexin V-FITC and PI was regarded as the negative control. A total of 10 fields-of-view were randomly selected under the high-power microscope, and the apoptosis rate was calculated according to the formula of $N_{apoptotic\ cells}/N_{total\ cells}$ x 100%.

Detection of tumor necrosis factor α (TNF-α), interleukin-6 (IL-6) and nitric oxide (NO) levels by ELISA. ELISA detection kits were used to determine the levels of TNF-α (cat. no. 88-7340-22 Thermo Fisher Scientific, Inc.), IL-6 (cat. no. RAB0308 Sigma-Aldrich; Merck KGaA) and NO (cat. no. A013-2, Nanjing Jiancheng Bio-Engineering Institute Co., Ltd., Nanjing, China), according to the manufacturer's protocol. The absorbance values at 450 and 520 nm were obtained, and the respective contents of TNF-α, IL-6 and NO were confirmed according to the standard curves.

Statistical analysis. The measurement data (mean ± standard deviation) were compared based on t-test, while multigroup comparisons were examined using analysis of variance, followed by Bonferroni's post-hoc test. Statistical analyses were conducted using SPSS 16.0 software (SPSS, Inc., Chicago, IL, USA). P<0.05 was considered to indicate a statistically significant difference.

Results

Establishment of AD cell model. As tau (S404) and tau (T231) are two major forms of phosphorylated tau, they were detected in the present study to demonstrate the abundance of phosphorylated tau within cells. It was revealed that the total tau and P-tau expressions were significantly elevated in the $A\beta_{25-35}$ treatment group in comparison with those in the control group (P<0.05; Fig. 1), indicating that the AD cell model was successfully constructed.

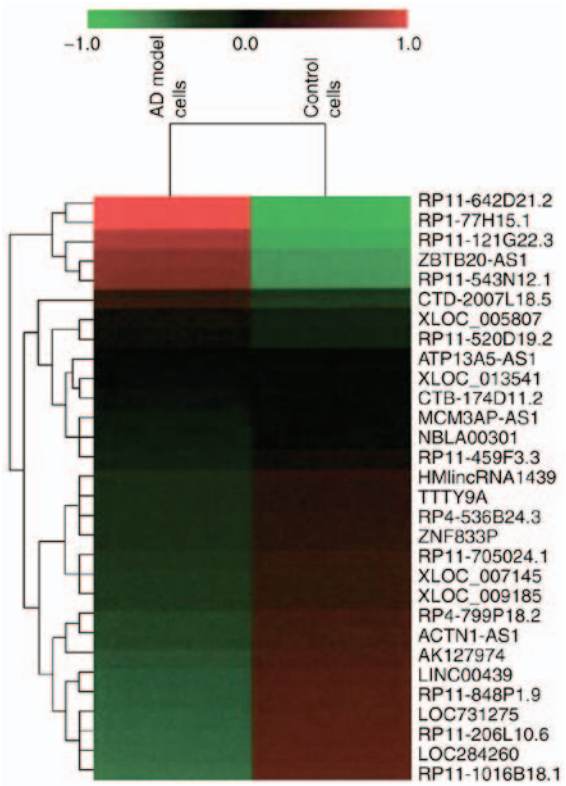

Figure 2. Differentially expressed lncRNAs between AD cell model and normal cell were partly displayed based on hierarchical clustering. Higher lncRNA expression is indicated by a more intense red color, while lower lncRNA expression is indicated by a more intense green color. lncRNA, long non-coding RNA; AD, Alzheimer's disease.

Identification of differentially-expressed lncRNAs between AD and normal groups by chip data analysis. Through screening of differentially expressed lncRNAs and mRNAs based on fold change (>2.0), 997 upregulated lncRNAs and 1,653 downregulated lncRNAs were observed within AD cell model in comparison to normal cell (P<0.05; Fig. 2). Furthermore,

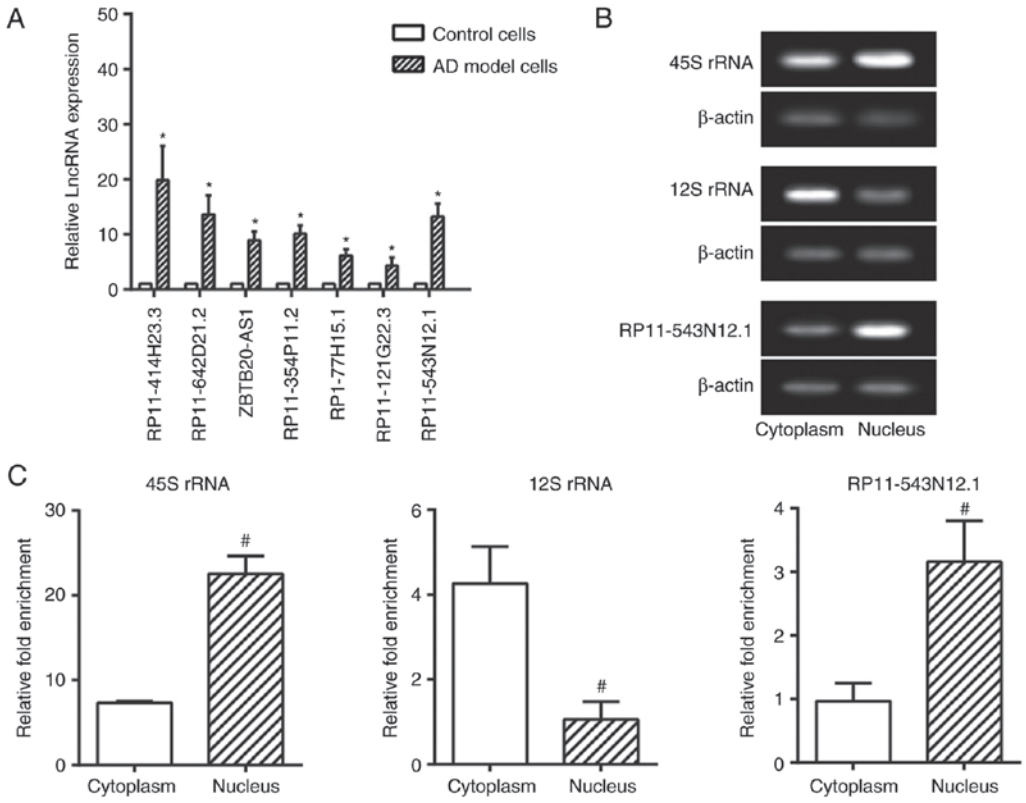

Figure 3. (A) Several lncRNAs that exhibited significantly distinct expression levels according to the chip results were determined by quantitative polymerase chain reaction. RP11-543N12.1 expression was compared between within the nucleus and cytoplasm by (B) western blot analysis and (C) densitometry. *P<0.05 vs. the respective control group; #P<0.05 vs. the cytoplasmic level. lncRNA, long non-coding RNA.

the expression levels of the lncRNAs RP11-414H23.3, RP11-642D21.1, ZBTB20-AS1, RP11-354P11.2, RP1-77H15.1, RP11-121G22.3 and RP11-543N12.1 were confirmed to differ significantly between the AD cell model and control cell (P<0.05) (Fig. 3A). Among them, lncRNA RP11-414H23.3 revealed the highest levels of expression; however, expression was deemed to be unstable within SH-SY5Y cells. Therefore, RP11-543N12.1 was selected for genetic sequencing and subsequent experiments, considering its relatively high and stable expression within AD cell models.

Sub-location of RP11-543N12.1 within SH-SY5Y cells. As displayed in Fig. 3B and C, the nuclear/cytoplasmic ratio of RP11-543N12.1 expression within 45S rRNA was greater compared with that within 12S rRNA (P<0.05), and the RP11-543N12.1 expression within the nucleus also exceeded that within the cytoplasm (P<0.05). Thus, it was suggested that RP11-543N12.1 may function mainly through modulating genetic transcriptions within the cell nucleus.

RP11-543N12.1 and Aβ25-35 coordinately facilitated miR-324-3p expression. Three siRNA interference sequences (i.e, siRNA-1#, siRNA-2# and siRNA-3#) were initially designed to ensure successful interference with lncRNA RP11-543N12.1. The results revealed that only siRNA-1# and siRNA-3# posed significant interfering effects, while the effect of siRNA-1# on lncRNA RP11-543N12.1 was more evident than that of siRNA-3# (Fig. 4A). Thus, siRNA-1# was selected for use in subsequent experiments.

In addition, the expression levels of miR-324-3p within the MOCK+Aβ_{25-35} and NC+Aβ_{25-35} groups were significantly higher than those with in MOCK and NC groups, respectively (P<0.05; Fig. 4B). Additionally, when the lncRNA RP11-543N12.1-siRNA1# group was treated with Aβ_{25-35}, its miR-324-3p expression was significantly lower than MOCK+Aβ_{25-35} and NC+Aβ_{25-35} groups, yet higher than MOCK and NC groups (Fig. 4B). Furthermore, transfection with pcDNA3.1(+)-RP11-543N12.1 vectors revealed significantly increased RP11-543N12.1 expression levels than the MOCK and pcDNA3.1(+) groups (P<0.05) (Fig. 4C), and the miR-324-3p expressions within pcDNA3.1(+)-RP11-543N12.1 and pcDNA3.1(+)-RP11-543N12.1+Aβ_{25-35} groups were also significantly increased compared with in the MOCK and pcDNA3.1(+) groups (P<0.05; Fig. 4D). Furthermore, as the miR-324-3p expression levels of the pcDNA3.1(+)-RP 11-543N12.1+Aβ_{25-35} group significantly exceeded that of the MOCK+Aβ_{25-35} group (P<0.05), it was suggested that Aβ_{25-35} and pcDNA3.1(+)-RP11-543N12.1 may upregulated miR-324-3p expression in a synergistic manner.

Targeted association between lncRNA RP11-543N12.1 and miR-324-3p. The miRDB 4.0 and PITA databases were used to co-predict the target miRNAs of RP11-543N12.1. It was observed that miR-324-3p was complementary to RP11-543N12.1, with a reasonable target score and target rank (Fig. 5A). In addition, the relative luciferase activity of the RP11-543N12.1-wt+miR-324-3p group was significantly suppressed (P<0.05), while the

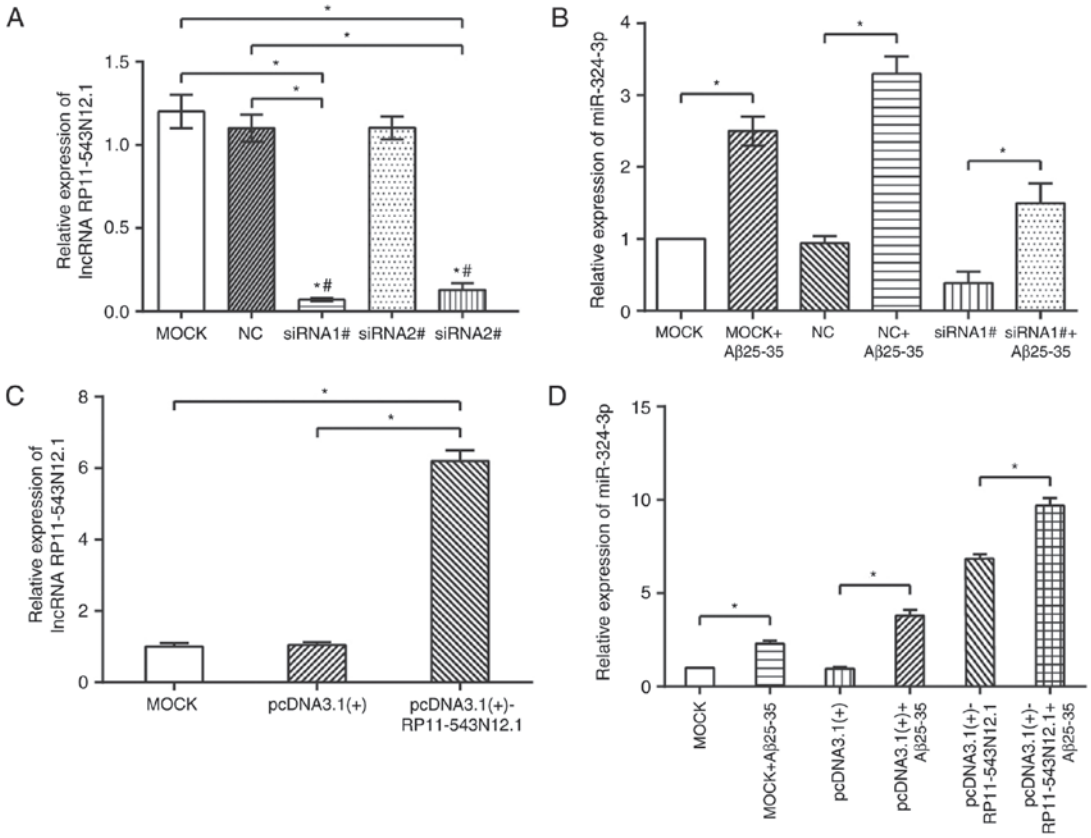

Figure 4. Relative expression levels of (A) lncRNA RP11-543N12 and (B) miR-324-3p were determined following transfection with lncRNA RP11-543N12.1-siRNAs. (C) lncRNA RP11-543N12 and (D) miR-324-3p relative expression levels were also determined following transfection with pcDNA3.1(+)-RP11-543N12.1. *P<0.05. lncRNA, long non-coding RNA; siRNA, small interfering RNA; miR, microRNA; Aβ, amyloid β.

RP11-543N12.1-mut+miR-324-3p group exhibited no evident difference when compared with the psiCHECK-2+miR-324-3p group, implying that RP11-543N12.1-wt was able to effectively bind to miR-324-3p (Fig. 5B).

RP11-543N12.1, miR-324-3p and MI contribute to reduction of cell viability and promotion of cell apoptosis. The results derived of the MTT assay (Fig. 6A) revealed that the cell activity of the MOCK+$A\beta_{25-35}$ and NC+$A\beta_{25-35}$ groups was significantly inhibited compared with in the MOCK and NC groups, respectively (P<0.05). Additionally, the cell viability of the $A\beta_{25-35}$+MI group was significantly reduced compared with in the NC+MI group (P<0.05; Fig. 6A). The dual treatments of RP11-543N12.1-siRNA1# and $A\beta_{25-35}$ (RP11-543N12.1-siRNA1#+$A\beta_{25-35}$ group) significantly increased cell viability compared with in MOCK+$A\beta_{25-35}$ or NC+$A\beta_{25-35}$ group (P<0.05); however, the RP11-543N12.1-siRNA1#+$A\beta_{25-35}$+MI group exhibited significantly lowered cell viability compared with in the RP11-543N12.1-siRNA1#+$A\beta_{25-35}$ group (P<0.05; Fig. 6A). On the contrary, the pcDNA3.1(+)-RP11-543N12.1+$A\beta_{25-35}$ group exhibited significantly reduced cell viability when compared with in MOCK+$A\beta_{25-35}$ or pcDNA3.1(+)+$A\beta_{25-35}$ group (P<0.05; Fig. 6B). In addition, the cell viability of the pcDNA3.1(+)-RP11-543N12.1+$A\beta_{25-35}$+MI group was significantly lower than that of the pcDNA3.1(+)-RP11-543N12.1+$A\beta_{25-35}$ group (P<0.05; Fig. 6B). Thus, it was suggested that RP11-543N12.1 may promote the inhibiting effects of $A\beta_{25-35}$ on cell viability, and that MI may enhance the inhibitory effects of $A\beta_{25-35}$ exerted on cell viability.

Similarly, transfection with miR-324-3p inhibitor followed by the addition of $A\beta_{25-35}$ for 48 h demonstrated significant increases in cell viability compared with in the NC+$A\beta_{25-35}$ group (P<0.05), yet the miR-324-3p inhibitor+$A\beta_{25-35}$+MI group exhibited significantly decreased cell viability than that of the miR-324-3p inhibitor+$A\beta_{25-35}$ group (P<0.05; Fig. 6C). Transfection with miR-324-3p mimic affected the cell ability in a manner that was contrary to that miR-324-3p inhibitor alone (P<0.05; Fig. 6D). Thus, it was hypothesized that the effects of MI and inhibited miR-324-3p expression may act in a synergic manner as for their roles in the reduced ability of SH-SY5Y cells induced by $A\beta_{25-35}$.

RP11-543N12.1, miR-324-3p and MI led to promoted cell apoptosis. For the cell groups transfected with RP11-543N12.1-siRNA, the apoptotic rate of the MOCK+$A\beta_{25-35}$ and NC+$A\beta_{25-35}$ groups appeared to exceed that of the MOCK and NC groups, respectively (P<0.05; Fig. 7A). In addition, the apoptotic rate of siRNA1#+$A\beta_{25-35}$ group was significantly lower than that of the MOCK+$A\beta_{25-35}$ group (P<0.05); the apoptotic rate of siRNA1#+$A\beta_{25-35}$+MI group was significantly upregulated compared with in the siRNA1#+$A\beta_{25-35}$ group (P<0.05; Fig. 7A). In contrast, the pcDNA3.1(+)-RP11-543N12.1+$A\beta_{25-35}$ group was associated with a significantly higher apoptotic rate than that of the MOCK+$A\beta_{25-35}$ group (P<0.05); the pcDNA3.1(+)-RP11-543N

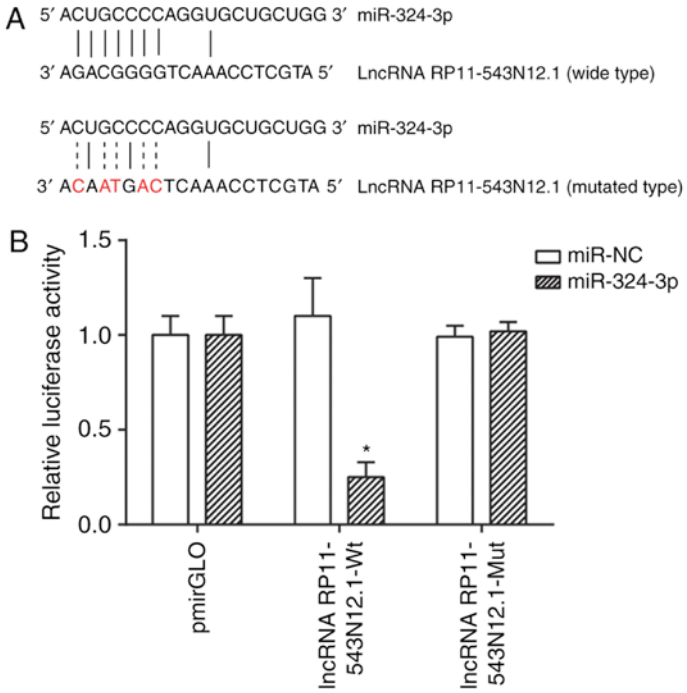

Figure 5. (A) The lncRNA RP11-543N12 targeted miR-324-3p as observed by the binding sites. (B) lncRNA RP11-543N12-wt, rather than its mut vector, exhibited a marked induction by miR-324-3p. *P<0.05 vs. the respective control group. lncRNA, long non-coding RNA; miR, microRNA; wt, wild-type; mut, mutated.

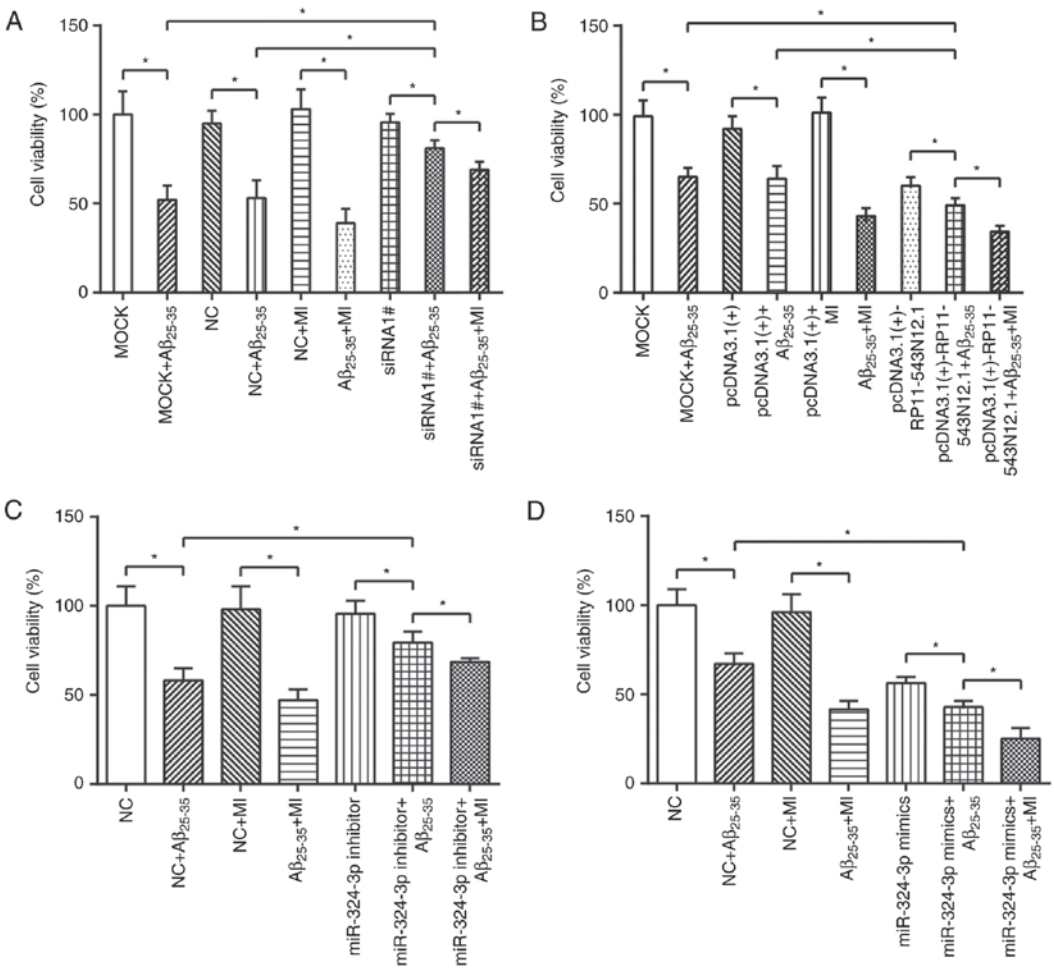

Figure 6. An MTT assay was employed to evaluate the effects of (A) lncRNA RP11-543N12.1-siRNA-1, (B) pcDNA3.1(+)-RP11-543N12.1, (C) miR-324-3p inhibitor and (D) miR-324-3p mimic on the viability of SH-SY5Y cells. *P<0.05. lncRNA, long non-coding RNA; siRNA, small interfering RNA; miR, microRNA; Aβ, amyloid β; MI, microglia.

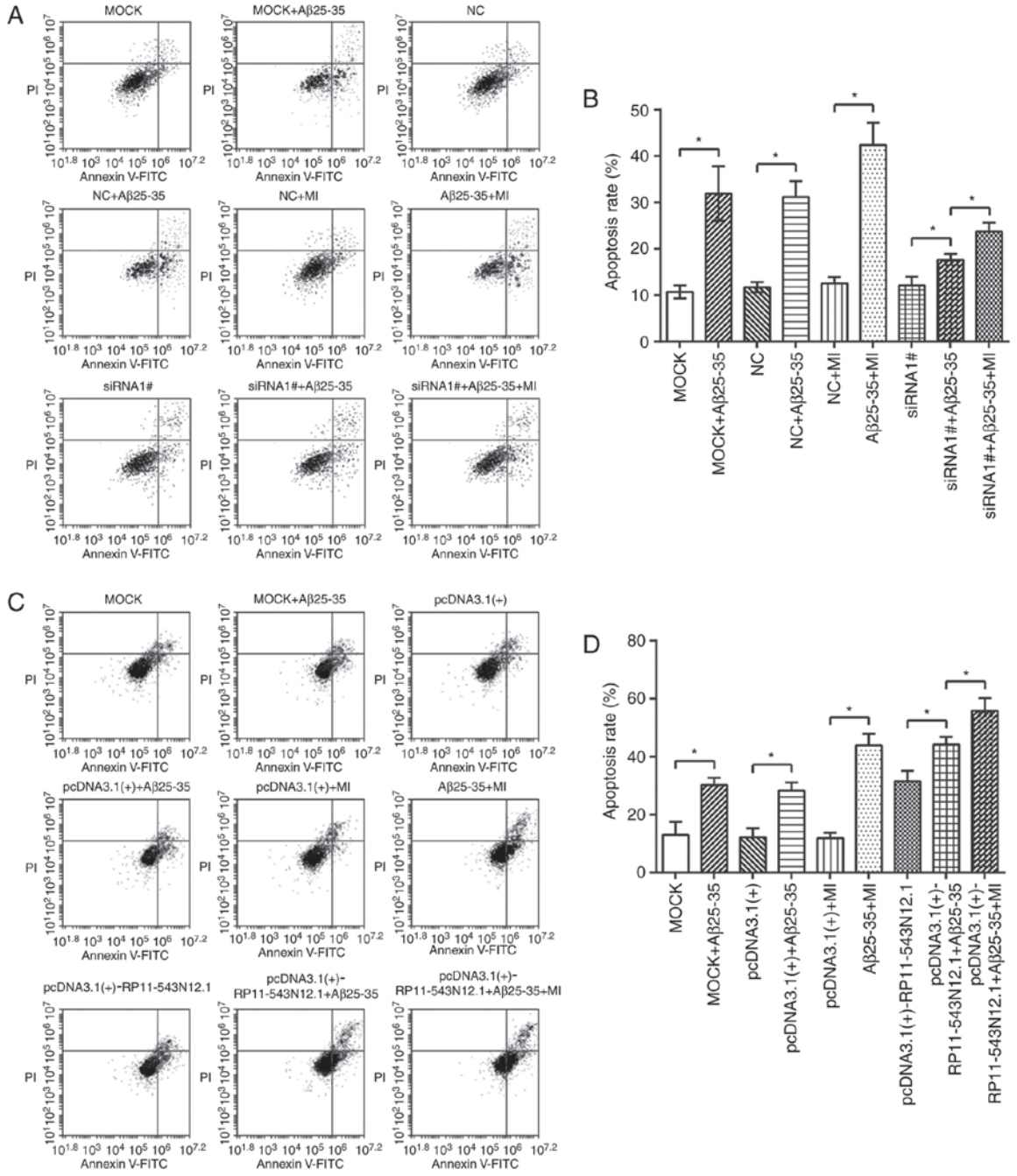

Figure 7. Flow cytometry was conducted to assess the effects of lncRNA RP11-543N12.1-siRNA-1 and pcDNA3.1(+)-RP11-543N12.1 on the apoptotic status of SH-SY5Y cells. (A) Flow cytometry graphs and (B) apoptosis rate in the cells transfected with siRNA. (C) Flow cytometry graphs and (D) apoptosis rate in the cells treated with pcDNA3.1(+)-RP11-543N12.1. *P<0.05. lncRNA, long non-coding RNA; siRNA, small interfering RNA; Aβ, amyloid β; MI, microglia.

12.1+$A\beta_{25-35}$+MI group exhibited significantly increased rates of apoptosis compared with in the pcDNA3.1(+)-RP11-543N12 .1+$A\beta_{25-35}$ group (P<0.05; Fig. 7B). Furthermore, the apoptotic rate of miR-324-3p inhibitor+$A\beta_{25-35}$ group was significantly higher than that of NC group (P<0.05); the miR-324-3p inhibitor+$A\beta_{25-35}$+MI group exhibited significantly increased apoptotic rates compared with in miR-324-3p inhibitor+$A\beta_{25-35}$ group (P<0.05; Fig. 8A). Additionally, miR-324-3p mimic+$A\beta_{25-35}$+MI group exhibited significantly enhanced apoptosis rate compared with the miR-324-3p mimic+$A\beta_{25-35}$ group; however, notable increase was observed compared with in the $A\beta_{25-35}$+MI group (P<0.05; Fig. 8B).

Effects of RP11-543N12.1 and miR-324-3p on the expressions of apoptosis-associated proteins. Increases in p53 and Bax expression levels, as well as reduced Bcl-2 expressions levels were observed in the MOCK+$A\beta_{25-35}$ and NC+$A\beta_{25-35}$ groups compared with in the MOCK and NC groups (P<0.05; Fig. 9A-F). Also, compared with in the MOCK+$A\beta_{25-35}$ group, the siRNA1#+$A\beta_{25-35}$ group revealed significantly elevated the Bcl-2 expression levels; p53 and Bax expression levels were significantly decreased (P<0.05; Fig. 9A-C). However, the pcDNA3.1(+)-RP11-543N12.1+$A\beta_{25-35}$ group revealed significantly downregulated Bcl-2 expression and upregulated p53 expression compared with in the MOCK+$A\beta_{25-35}$

Table II. Secretion level of inflammatory molecules (TNF-α, IL-6 and NO) affected by MI and Aβ25-35.

Group	TNF-α (ng/ml)	IL-6 (pg/ml)	NO (μmol/l)
Control	3.39±0.39	9.67±3.05	2.69±0.54
Aβ25-35+MI	32.78±2.21[a]	204.16±19.44[a]	40.64±3.16[a]
RP11-543N12.1-siRNA-1 + Aβ25-35+MI	4.56±0.78	9.12±2.45	3.01±0.82
pcDNA3.1(+)-RP11-543N12.1 + Aβ25-35+MI	47.23±3.25[a]	284.32±22.78[a]	55.85±6.13[a]
miR-324-3p inhibitor + Aβ25-35+MI	5.12±0.47[a]	11.03±1.98	4.93±0.75[a]
miR-324-3p mimics + Aβ25-35+MI	43.63±2.94[a]	253.89±19.78[a]	49.71±7.31[a]

MI, microglia; Aβ, amyloid β; miR, microRNA; TNF, tumor necrosis factor; IL, interleukin; NO, nitric oxide. [a]P<0.05 vs. control group.

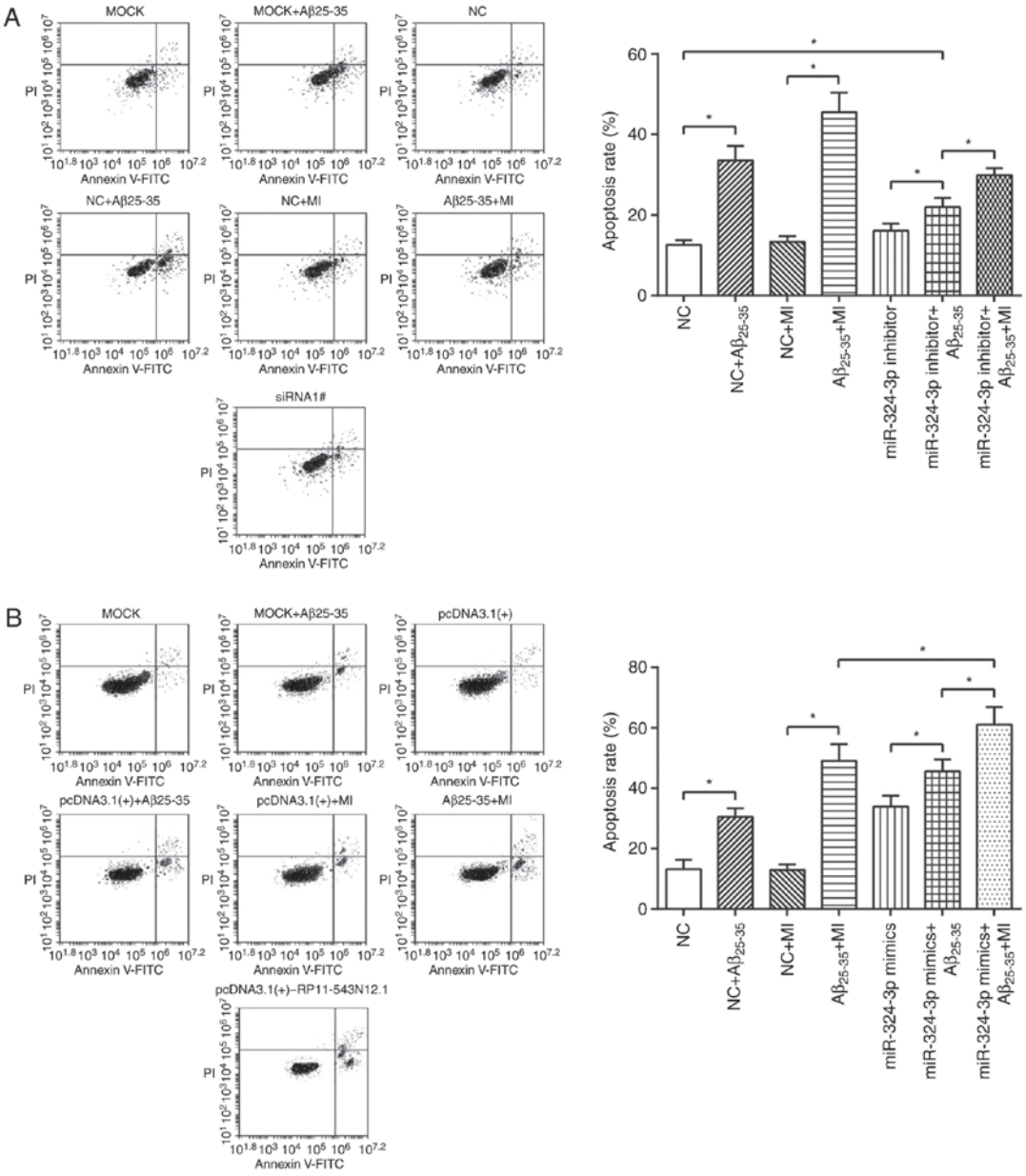

Figure 8. Flow cytometry was conducted to assess the effects of miR-324-3p inhibitor and miR-324-3p mimics on the apoptotic status of SH-SY5Y cells. (A) Flow cytometry graphs and apoptosis rate in inhibitor-treated cells. (B) Flow cytometry graphs and apoptosis rate in mimic-treated cells. *P<0.05. miR, microRNA; Aβ, amyloid β; MI, microglia.

group(P<0.05) (Fig. 9D-F). Furthermore, the addition of MI significantly (siRNA1#+$A\beta_{25\text{-}35}$+MI group) reversed the effects of siRNA1# (siRNA1#+$A\beta_{25\text{-}35}$ group) on the expression of apoptosis-associated proteins, upregulating

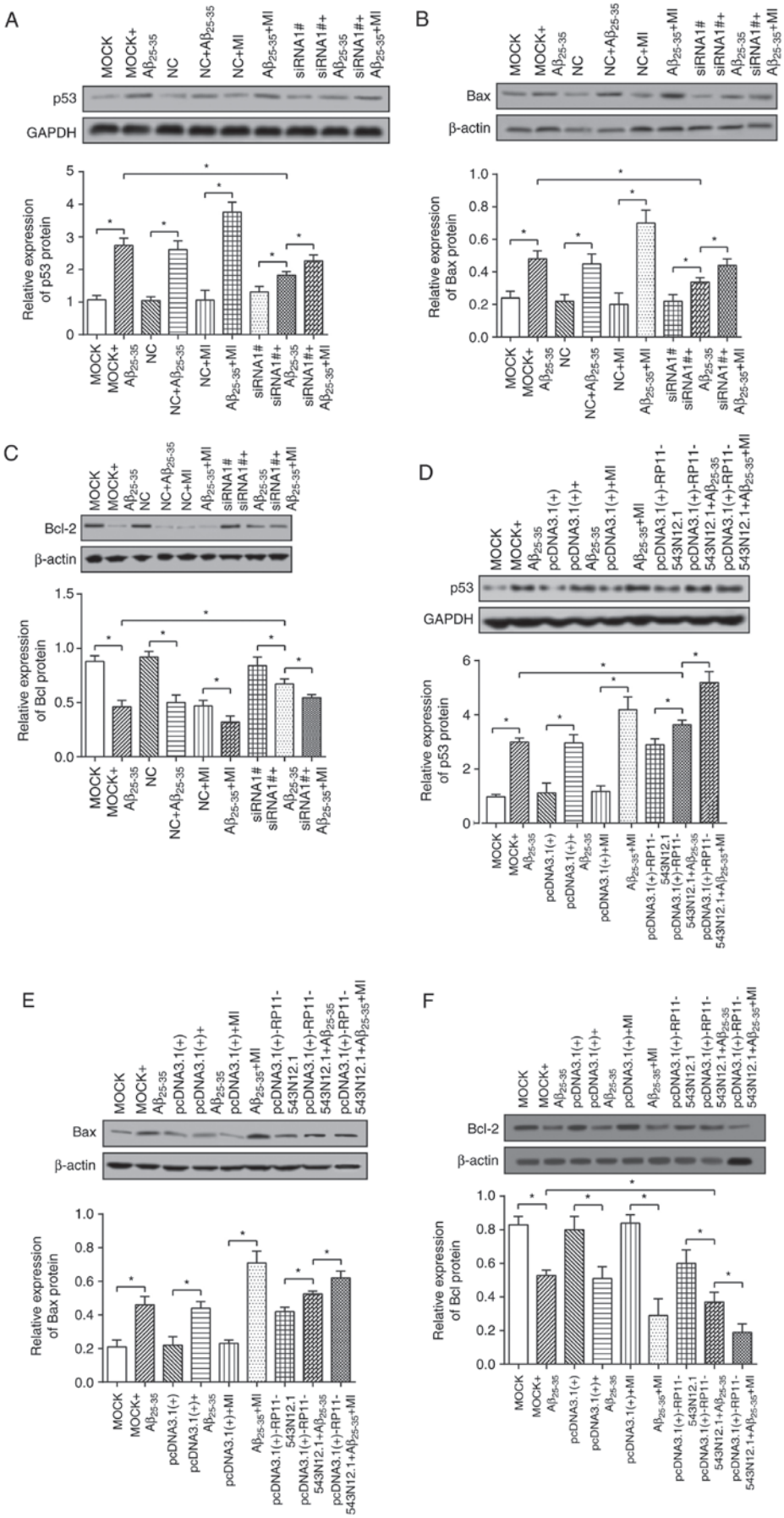

Figure 9. Regulatory role of the lncRNA RP11-543N12.1-siRNA-1 and pcDNA3.1(+)-RP11-543N12.1 on the expression levels of apoptosis-associated proteins, as detected by western blot analysis. Effect of (A) siRNA and (D) pcDNA3.1(+)-RP11-543N12.1 on p53 levels; effect of (B) siRNA and (E) pcDNA3.1(+)-RP11-543N12.1 on Bax levels; effect of (C) siRNA and (F) pcDNA3.1(+)-RP11-543N12.1 on Bcl-2 levels. *P<0.05. lncRNA, long non-coding RNA; siRNA, small interfering RNA; Aβ, amyloid β; MI, microglia; Bcl-2, B-cell lymphoma 2; Bax, Bcl-2-associated X protein.

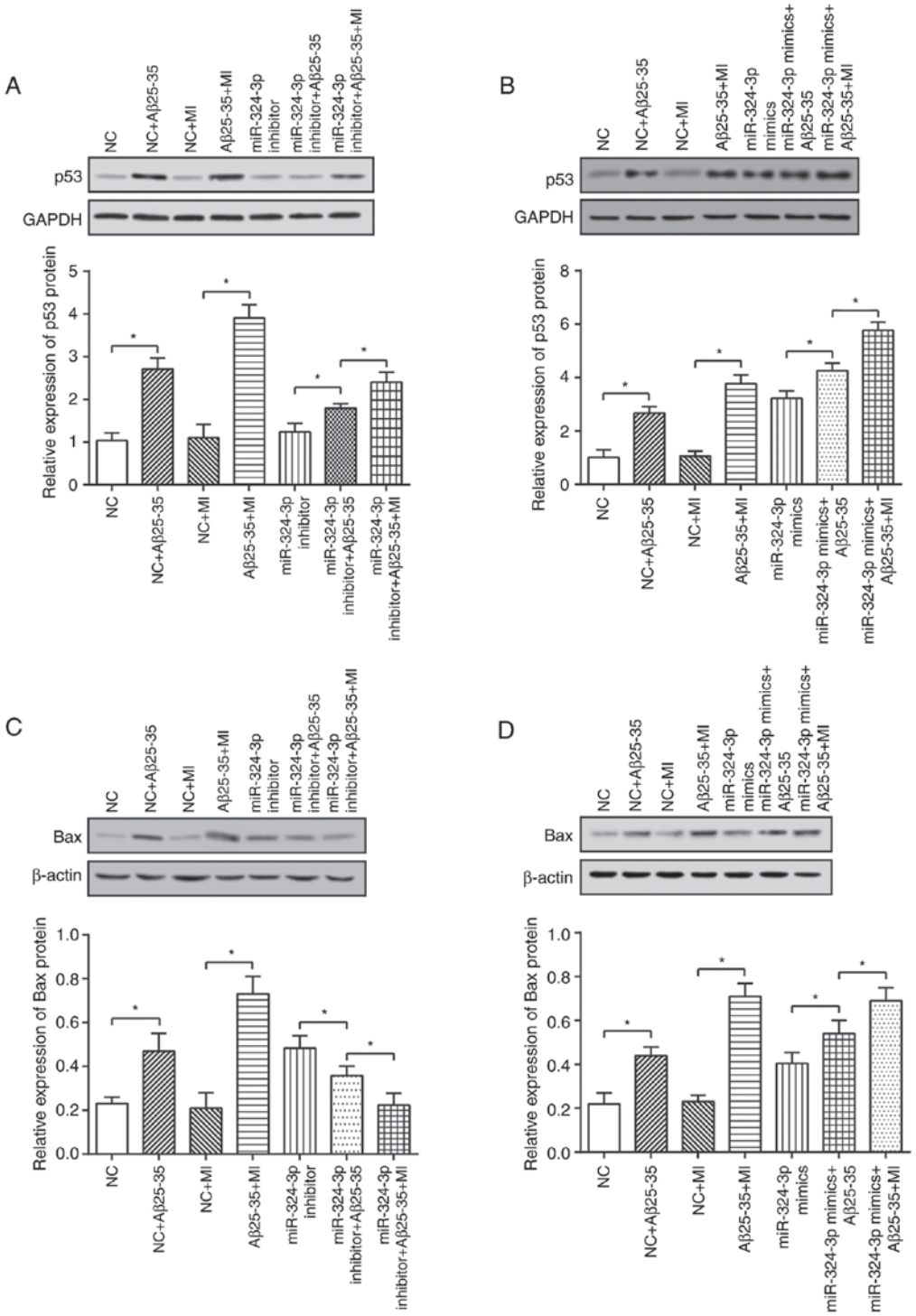

Figure 10. Regulatory role of miR-324-3p inhibitor and miR-324-3p mimics on the expression of apoptosis-associated proteins. Effect of (A) miR-324-3p inhibitor and (B) miR-324-3p mimics on p53 levels; effect of (C) inhibitor and (D) mimics on Bax levels..

p53/Bax expression levels and downregulating Bcl-2 expression levels (P<0.05).

In addition, the miR-324-3p inhibitor+A$\beta_{25\text{-}35}$ group was exhibited significantly reduced p53 and Bax expression levels, as well as increased Bcl-2 expression levels compared with in the NC+A$\beta_{25\text{-}35}$ group (P<0.05; Fig. 10A-C). Furthermore, the miR-324-3p mimic+A$\beta_{25\text{-}35}$ group exhibited increased p53 and Bax expressions, along with decreased Bcl-2 expressions compared with in the NC+A$\beta_{25\text{-}35}$ group as the control (P<0.05; Fig. 10D-F).

Overexpression of RP11-543N12.1 and miR-324-3p further elevates the ability of MI to secrete inflammatory molecules within SH-SY5Y cells. Under the stimulation of A$\beta_{25\text{-}35}$, the secretion levels of TNF-α, IL-6 and NO in the supernatants of the activated MI culture solution increased from 3.39 to 32.78 ng/ml, from 9.67 to 204.16 pg/ml, and from 2.69 to 40.64 μmol/l, respectively (P<0.05). The levels of TNF-α, IL-6 and NO secreted by MI markedly dropped when co-cultured with SH-SY5Y cells transfected with RP11-543N12.1-siRNA or miR-324-3p inhibitor (P<0.05), although they remained

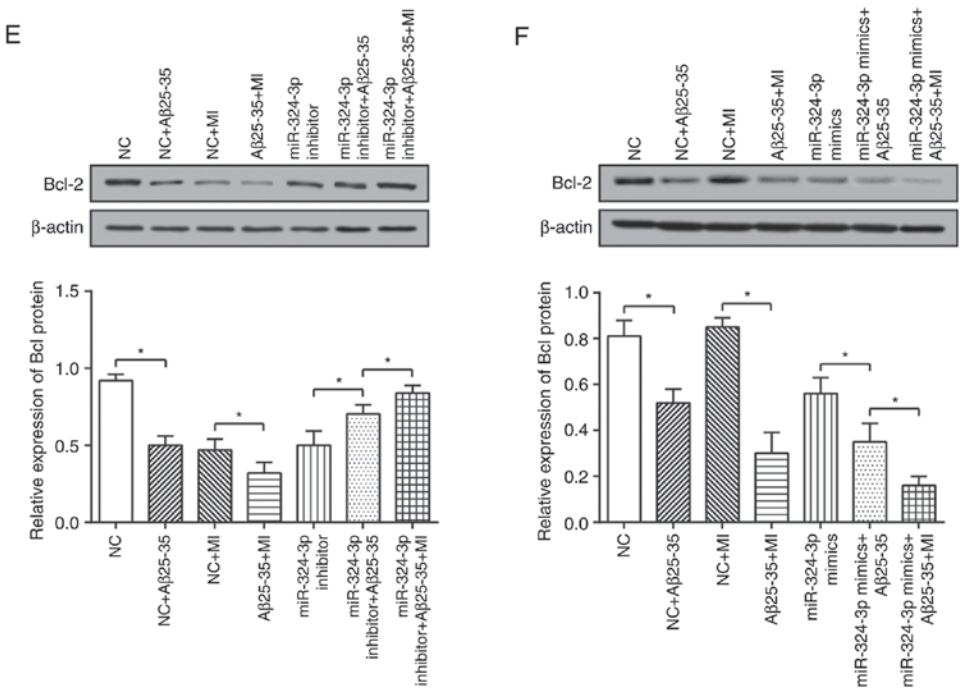

Figure 10. Continued. Regulatory role of miR-324-3p inhibitor and miR-324-3p mimics on the expressions of apoptosis-associated proteins. Effect of (E) inhibitor and (F) mimics on Bcl-2 levels.*P<0.05. miR, microRNA; Aβ, amyloid β; MI, microglia; Bcl-2, B-cell lymphoma 2; Bax, Bcl-2-associated X protein.

higher than those of the control group (Table II). By contrast, co-culturing with SH-SY5Y cells transfected with pcDNA3.1(+)-RP11-543N12.1 or miR-324-3p mimics enable further elevation of TNF-α, IL-6 and NO levels secreted by MI (P<0.05).

Discussion

A large number of studies have demonstrated that lncRNAs are involved in essential biological processes, including pluripotency maintenance, genomic imprinting and immune responses (23-25). Recently, specific lncRNAs were reported to serve a crucial role in the development of AD, for instance, the lncRNAs AP000265, KB-1460A1.5 and RP11-145M9.4 were identified to accelerate presence of intracellular neurofibrillary tangle, which is a major etiology of AD (26-28). In the present study, a cell model of AD was established through treating neuroblastoma SH-SY5Y cells with $A\beta_{25-35}$, and the successful construction of the AD cell model was verified by detecting the total tau and P-tau expression levels. Consistent with a previous study (29), the current microarray results demonstrated that RP11-543N12.1 was differentially expressed between $A\beta_{25-35}$-treated and control cells (P<0.05; Figs. 2 and 3).

lncRNAs have been demonstrated to compete with miRNA target genes by sharing common miRNA-binding sites, thereby relieving miRNA-mediated target inhibition (26). Similarly, in the present study, the targeted association of RP11-543N12.1 and miR-324-3p was predicted based on the miRDB4.0 and PITA databases, and a dual-luciferase reporter assay was conducted to elucidate relative mechanisms. As a consequence, the present study results indicated that miR-324-3p was a target gene of RP11-543N12.1, and that miR-324-3p expression was significantly increased upon the direct binding of RP11-543N12.1 to the 3'-untranslated region of miR-324-3p.

It was previously revealed that lncRNAs was able to regulate cell proliferation and apoptosis (30), while miR-324-3p is believed to be a multi-functional miRNA involved in the proliferation and apoptosis of cancer cells (31,32). More specifically, miR-324-3p participated in modulating the apoptotic status of nasopharyngeal carcinoma cells via targeting and upregulating the expression of downstream SMAD7 (31). In order to further ascertain the apoptosis-associated mechanisms of miR-324-3p and RP11-543N12.1 within AD cells, pcDNA3.1(+)-RP11-543N12.1, miR-324-3p mimics, RP11-543N12.1-siRNA and miR-324-3p inhibitor were respectively transfected into SH-SY5Y cells in the present study. The finding revealed that upregulation of RP11-543N12.1 and miR-324-3p not only suppressed the proliferation of SH-SY5Y cells, but also promoted their apoptosis. By contrast, inhibition of RP11-543N12.1 and miR-324-3p expression increased SH-SY5Y cell proliferation and inhibited their apoptosis. Furthermore, the study identified that the co-culture of MI with SH-SY5Y cells that were transfected with pcDNA3.1(+)-RP11-543N12.1 or miR-324-3p mimics significantly enhanced the apoptosis of SH-SY5Y cells (P<0.05). Thus, these data indicated that the expression of miR-324-3p was modulated by RP11-543N12.1, and that RP11-543N12.1 was able to increase the apoptosis of SH-SY5Y cells by upregulating miR-324-3p.

Bcl-2 is a direct participant in cell apoptosis and has an anti-apoptotic effect (33). Previous studies have suggested that Bcl-2 was lowly expressed or even not expressed within apoptotic cells (34). The tumor suppressor p53 was reported to induce cell apoptosis by inhibition of Bcl-2 expression,

which was mediated by the direct binding of p53 to a negative portion that was beyond the range of the Bcl-2 promoter (35). Moreover, Bcl-2 promoted cell apoptosis, yet Bax contributed to decreased cell apoptosis (36). Therefore, these three molecules were selected to assess the apoptotic condition of SH-SY5Y cells in the current study. In agreement with the aforementioned studies, the current results indicated higher p53 and Bax activities, as well as increased apoptosis rate, in cells transfected with pcDNA3.1(+)-RP11-543N12.1 and miR-324-3p mimics. By contrast, lower p53 and Bax activities, accompanied with decreased apoptosis rate, were examined within cells transfected with pcDNA3.1(+)-RP11-543N12.1 and miR-324-3p mimics. Taken together, RP11-543N12.1 and miR-324-3p served as two parameters promoting the apoptosis of SH-SY5Y cells, which is a crucial step in the facilitation of AD onset.

As previously reported, chronic or sustained inflammatory signaling usually contribute to multiple pathological and degenerative conditions, including AD and cancer (37). In addition, MI responds to AD-relevant Aβ by releasing pro-inflammatory factors (such as NO, reactive oxygen species and prostaglandin E2), cytokines (such as TNF-α, IL-1β and IL-6), and chemotactic factors that attract monocytes and T-cells to the inflammation region (38). In the present study, the expression levels of TNF-α, IL-6 and NO were higher when MI cells were co-cultured with RP11-543N12.1- or miR-324-3p-overexpressing SH-SY5Y cells, verifying that RP11-543N12.1 participated in the MI-mediated inflammatory pathway by binding to miR-324-3p.

In conclusion, the present study revealed that RP11-543N12.1 inhibited the proliferation and promoted the apoptosis of an AD cell model through positively regulating miR-324-3p. It is thus suggested that RP11-543N12.1 and miR-324-3p may serve as effective biomarkers and therapeutic targets for AD in the future. However, only an AD cell model was used in the current study, therefore, it is highly recommended that animal models are also established to validate the aforementioned mechanism. Simultaneously, clinical specimens should be gathered to verify whether RP11-543N12.1 and miR-324-3p follow the tendencies suggested by the microarray analysis. Ultimately, further direct associations among the lncRNA RP11-543N12.1/miR-324-3p axis, MIs and SH-SY5Y cells may be explored in the future; thus, whether the inflammatory factors secreted by MI cells affect the transcription of specific lncRNAs, miRNAs or mRNAs should be further investigated.

Acknowledgements

Not applicable.

Funding

This study was supported by the Public Welfare Project from the Science Technology Department of Zhejiang Province (grant no. 2015C33135).

Availability of data and materials

All data generated or analyzed during this study are included in this article.

Authors' contributions

MC, YW and SX conceived and designed the experiments. MC, YW, SX, SQ, QS, JD, YL and XL performed the experiments. SQ, QS and JD analyzed the data. YL and XL drafted the manuscript. All authors read and approved the final manuscript.

Ethics approval and consent to participate

All participants provided written informed consent. The present study was approved by the Ethics committee of Zhejiang Hospital (Hangzhou, China).

Patient consent for publication

Not applicable.

Competing interests

The authors declare that they have no competing interests.

References

1. D'Amore JD, Kajdasz ST, McLellan ME, Bacskai BJ, Stern EA and Hyman BT: In vivo multiphoton imaging of a transgenic mouse model of Alzheimer disease reveals marked thioflavine-S-associated alterations in neurite trajectories. J Neuropathol Exp Neurol 62: 137-145, 2003.
2. Yoshiyama Y, Higuchi M, Zhang B, Huang SM, Iwata N, Saido TC, Maeda J, Suhara T, Trojanowski JQ and Lee VM: Synapse loss and microglial activation precede tangles in a P301S tauopathy mouse model. Neuron 53: 337-351, 2007.
3. Lemere CA, Maier M, Jiang L, Peng Y and Seabrook TJ: Amyloid-beta immunotherapy for the prevention and treatment of Alzheimer disease: Lessons from mice, monkeys, and humans. Rejuvenation Res 9: 77-84, 2006.
4. Galimberti D and Scarpini E: Progress in Alzheimer's disease. J Neurol 259: 201-211, 2012.
5. Alzheimer's Association: 2010 Alzheimer's disease facts and figures. Alzheimers Dement 6: 158-194, 2010.
6. Millan MJ: Linking deregulation of non-coding RNA to the core pathophysiology of Alzheimer's disease: An integrative review. Prog Neurobiol 156: 1-68, 2017.
7. Qi X, Shao M, Sun H, Shen Y, Meng D and Huo W: Long non-coding RNA SNHG14 promotes microglia activation by regulating miR-145-5p/PLA2G4A in cerebral infarction. Neuroscience 348: 98-106, 2017.
8. Lin ST, Heng MY, Ptáček LJ and Fu YH: Regulation of myelination in the central nervous system by nuclear lamin B1 and non-coding RNAs. Transl Neurodegener 3: 4, 2014.
9. Liu X, Hou L, Huang W, Gao Y, Lv X and Tang J: The mechanism of long non-coding RNA MEG3 for neurons apoptosis caused by hypoxia: Mediated by miR-181b-12/15-LOX signaling pathway. Front Cell Neuroscie 10: 201, 2016.
10. Ko CY, Chu YY, Narumiya S, Chi JY, Furuyashiki T, Aoki T, Wang SM, Chang WC and Wang JM: CCAAT/enhancer-binding protein delta/miR135a/thrombospondin 1 axis mediates PGE2-induced angiogenesis in Alzheimer's disease. Neurobiol Aging 36: 1356-1368, 2015.
11. Zhao Y, Bhattacharjee S, Jones BM, Dua P, Alexandrov PN, Hill JM and Lukiw WJ: Regulation of TREM2 expression by an NF-κB-sensitive miRNA-34a. Neuroreport 24: 318-323, 2013.
12. Jayadev S, Case A, Alajajian B, Eastman AJ, Möller T and Garden GA: Presenilin 2 influences miR146 level and activity in microglia. J Neurochem 127: 592-599, 2013.
13. Dharap A, Pokrzywa C, Murali S, Pandi G and Vemuganti R: MicroRNA miR-324-3p induces promoter-mediated expression of RelA gene. PLoS One 8: e79467, 2013.
14. Gutierrez H, O'Keeffe GW, Gavaldà N, Gallagher D and Davies AM: Nuclear factor kappa B signaling either stimulates or inhibits neurite growth depending on the phosphorylation status of p65/RelA. J Neurosci 28: 8246-8256, 2008.

15. Peng Y, Gallagher SF, Landmann R, Haines K and Murr MM: The role of p65 NF-kappaB/RelA in pancreatitis-induced Kupffer cell apoptosis. J Gastrointest Surg 10: 837-847, 2006.
16. Sheehy AM and Schlissel MS: Overexpression of RelA causes G1 arrest and apoptosis in a pro-B cell line. J Biol Chem 274: 8708-8716, 1999.
17. Shankar GM, Li S, Mehta TH, Garcia-Munoz A, Shepardson NE, Smith I, Brett FM, Farrell MA, Rowan MJ, Lemere CA, *et al*: Amyloid-beta protein dimers isolated directly from Alzheimer's brains impair synaptic plasticity and memory. Nat Med 14: 837-842, 2008.
18. McGeer EG and McGeer PL: Inflammatory processes in Alzheimer's disease. Prog Neuropsychopharmacol Biol Psychiatry 27: 741-749, 2003.
19. Dobrenis K: Microglia in cell culture and in transplantation therapy for central nervous system disease. Methods 16: 320-344, 1998.
20. Tan AM, Zhao P, Waxman SG and Hains BC: Early microglial inhibition preemptively mitigates chronic pain development after experimental spinal cord injury. J Rehabil Res Dev 46: 123-133, 2009.
21. Roth R, Madhani HD and Garcia JF: Total RNA isolation and quantification of specific RNAs in fission yeast. Methods Mol Biol 1721: 63-72, 2018.
22. Livak KJ and Schmittgen TD: Analysis of relative gene expression data using real-time quantitative PCR and the $2^{-\Delta\Delta C_T}$ method. Methods 25: 402-408, 2001.
23. Mercer TR, Dinger ME and Mattick JS: Long non-coding RNAs: Insights into functions. Nat Rev Genet 10: 155-159, 2009.
24. Wu P, Zuo X, Deng H, Liu X, Liu L and Ji A: Roles of long noncoding RNAs in brain development, functional diversification and neurodegenerative diseases. Brain Res Bull 97: 69-80, 2013.
25. Batista PJ and Chang HY: Long noncoding RNAs: Cellular address codes in development and disease. Cell 152: 1298-1307, 2013.
26. Wang LK, Chen XF, He DD, Li Y and Fu J: Dissection of functional lncRNAs in Alzheimer's disease by construction and analysis of lncRNA-mRNA networks based on competitive endogenous RNAs. Biochem Biophys Res Commun 485: 569-576, 2017.
27. Ciarlo E, Massone S, Penna I, Nizzari M, Gigoni A, Dieci G, Russo C, Florio T, Cancedda R and Pagano A: An intronic ncRNA-dependent regulation of SORL1 expression affecting Aβ formation is upregulated in post-mortem Alzheimer's disease brain samples. Dis Model Mech 6: 424-433, 2013.
28. Mus E, Hof PR and Tiedge H: Dendritic BC200 RNA in aging and in Alzheimer's disease. Proc Natl Acad Sci USA 104: 10679-10684, 2007.
29. Zhou X and Xu J: Identification of Alzheimer's disease-associated long noncoding RNAs. Neurobiol Aging 36: 2925-2931, 2015.
30. Yan B and Wang Z: Long noncoding RNA: Its physiological and pathological roles. DNA Cell Biol 31 (Suppl 1): S34-S41, 2012.
31. Xu J, Ai Q, Cao H and Liu Q: MiR-185-3p and miR-324-3p predict radiosensitivity of nasopharyngeal carcinoma and modulate cancer cell growth and apoptosis by targeting SMAD7. Med Sci Monit 21: 2828-2836, 2015.
32. Kuo WT, Yu SY, Li SC, Lam HC, Chang HT, Chen WS, Yeh CY, Hung SF, Liu TC, Wu T, *et al*: MicroRNA-324 in human cancer: miR-324-5p and miR-324-3p have distinct biological functions in human cancer. Anticancer Res 36: 5189-5196, 2016.
33. Liu N, Zheng Y, Zhu Y, Xiong S and Chu Y: Selective impairment of CD4+CD25+Foxp3+ regulatory T cells by paclitaxel is explained by Bcl-2/Bax mediated apoptosis. Int Immunopharmacol 11: 212-219, 2011.
34. Yang Q, Yang K and Li A: microRNA-21 protects against ischemia-reperfusion and hypoxia-reperfusion-induced cardiocyte apoptosis via the phosphatase and tensin homolog/Akt-dependent mechanism. Mol Med Rep 9: 2213-2220, 2014.
35. Miyashita T, Krajewski S, Krajewska M, Wang HG, Lin HK, Liebermann DA, Hoffman B and Reed JC: Tumor suppressor p53 is a regulator of bcl-2 and bax gene expression in vitro and in vivo. Oncogene 9: 1799-1805, 1994.
36. Moshrefi M, Spotin A, Kafil HS, Mahami-Oskouei M, Baradaran B, Ahmadpour E and Mansoori B: Tumor suppressor p53 induces apoptosis of host lymphocytes experimentally infected by Leishmania major, by activation of Bax and caspase-3: A possible survival mechanism for the parasite. Parasitol Res 116: 2159-2166, 2017.
37. Lukiw WJ: NF-κB-regulated, proinflammatory miRNAs in Alzheimer's disease. Alzheimers Res Ther 4: 47, 2012.
38. Lee M: Neurotransmitters and microglial-mediated neuroinflammation. Curr Protein Pept Sci 14: 21-32, 2013.